ACS OMEGA

Open Access

http://pubs.acs.org/journal/acsodf

Article

Corrosion Protection of Mild Steel in Acidic Environments by Cetrimonium Cinnamates in Solution and Added to a Low Volatile Organic Compound Coating

Diulia Quites Rodrigues, Mahdi Ghorbani, Jhonatan Soto Puelles, Simon Crawford, Maria Paulis,* Maria Forsyth, and Anthony E. Somers*

Cite This: *ACS Omega* 2025, 10, 18225−18237

Read Online

ACCESS | Metrics & More | Article Recommendations | Supporting Information

ABSTRACT: Protection of mild steel from acidic solutions used in the industry by environmentally friendly methods is an area of need. This work explores the anticorrosive properties of cetrimonium cinnamate compounds for mild steel in acid solutions as an additive in solution and as a pigment in a low-volatility organic compound (VOC) coating. Immersion tests show that protection is considerably enhanced after 24 h, at pH 1 i_{corr} for the control being 330 μA/cm^2 compared to 4.3 μA/cm^2 for CTA-MeOcinn, suggesting synergy between the cetrimonium cation and cinnamate anion systems. NMR and cryo-transmission electron microscopy (cryo-TEM) suggested entrapment of the cinnamate within the cetrimonium micelles. This is further supported by molecular dynamics (MD) simulations, which also show that the carboxylate groups on the cinnamate protrude from the cetrimonium micelles, enhancing the attachment to the surface. The inhibitors are incorporated into waterborne polymeric coatings and tested in solutions at pH 1. Electrochemical impedance spectroscopy (EIS) data show that the inhibitors form a protective barrier, significantly increasing pore and charge transfer resistances for the coating, thus demonstrating the use of safe methods to protect mild steel in acidic conditions.

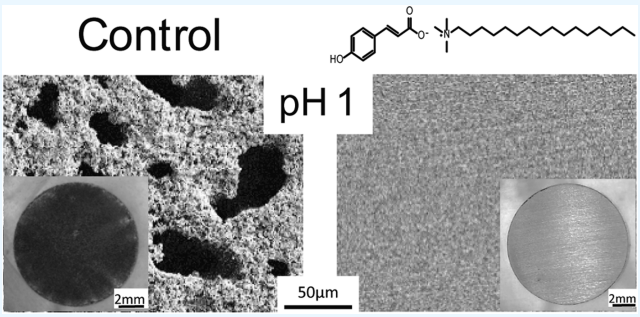

INTRODUCTION

The use of corrosion inhibitors is one of the most effective and inexpensive methods for mitigation of corrosion of metals and alloys, and this is particularly important in acidic conditions.[1−3] The most effective inhibitors historically used have often proven to be toxic, such as nitrites or those containing heavy metals like Pb(II,IV) and Cr VI; thus, there is a need for effective, nontoxic inhibitors.

Inhibitors are an attractive option for reducing corrosion due to their flexibility; they can be incorporated into paint coatings, added to water tanks, or continuously fed into pipelines or streams.[4−6] As an additive to paint coatings, they can continue to protect a surface even after the coating has been damaged by leaching out at the site of damage. Paint coatings are another area of environmental concern; most polymer coatings are sourced from nonrenewable materials, contain volatile organic compounds (VOCs), and are not readily broken down. Considering that many coated materials are in contact with natural environments (soil, aqueous, marine), their constituents (like VOCs) are destined to contribute significantly to the uncontrolled growth of microplastic pollution.

Unfortunately, it is proving extremely difficult to replace such inhibitor and coating systems with nontoxic counterparts that show a comparable level of performance, particularly in acidic conditions. In this study, the combination of a novel nontoxic inhibitor system with a low VOC coating is investigated to protect mild steel at low pH.

Conventional inhibitors are typically efficient for specific environmental conditions;[7] however, variations of temperature, pH, humidity, and salinity are likely to be found in industrial environments such as in the oil and chemical industry. Therefore, the development of environmental friendly compounds that could prevent the corrosion of mild steel in different conditions is desired.[2] An interesting approach is to combine components with different inhibitory properties into a single inhibitor compound for enhanced performance.[7] In previous works, we have studied the combination of carboxylates with both rare earth metals and different organic cationic inhibitors.[8−10] For instance, lanthanum 4-hydroxycinnamate has shown remarkable corrosion protection of mild

Received: August 2, 2024
Revised: February 21, 2025
Accepted: February 25, 2025
Published: April 30, 2025

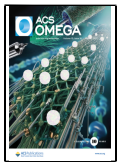

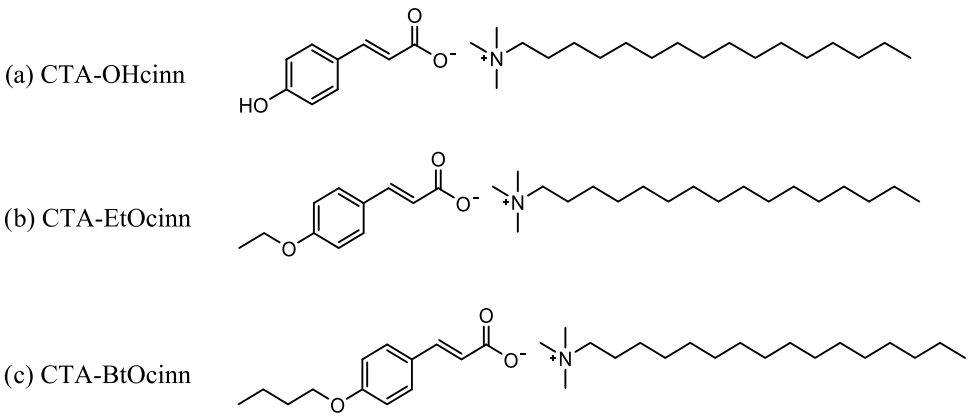

Figure 1. Chemical structure of (a) hexadecyl trimethylammonium bromide *trans*-4-butoxy-cinnamate (CTA-OHcinn), (b) hexadecyl trimethylammonium bromide *trans*-4-ethoxy-cinnamate (CTA-EtOcinn), and (c) hexadecyl trimethylammonium bromide *trans*-4-hydroxycinnamate (CTA-BtOcinn) inhibitors.

steel in 0.01 NaCl in a pH range from 2.5 to 8, being more effective at higher pH. The lower inhibition observed at acidic pH was attributed to a poor synergy between lanthanum chloride $[LaCl_4]^-$ and 4-hydroxycinnamic acid.[11] Following that, Chong et al. showed that the same anion, hydroxycinnamate, in combination with an imidazolinium cation can inhibit mild steel corrosion over a wide range of pH.[4] These studies revealed that such inhibitor compounds can act by suppressing both the anodic and cathodic reactions due to a synergistic effect leading to a higher efficiency.[7−9]

The commonly used antimicrobial surfactant cetyltrimethylammonium bromide (CTAB), also known as hexadecyl trimethylammonium bromide, or simplified to cetrimonium bromide, has previously been investigated as a corrosion inhibitor in acidic conditions,[12−14] showing promising performance. Through comparing different halide counterions, a mechanism of action is proposed whereby the halide is attracted to the surface, to which the surfactant then bonds. These surfactants are known to form micelles in solution, and researchers have shown that smaller organic counterions, such as salicylate, can be incorporated into the micelle structure and that this structure can change with pH.[15] Recently, this behavior was used to combine the corrosion-inhibiting 4-hydroxycinnamate anion (OHcinn) with the surface-active counterion, hexadecyl trimethylammonium, or cetrimonium (CTA) known for its biocidal[16] as well as anticorrosive properties in order to analyze if a synergistic behavior combining both properties could be achieved.[17] Results showed that CTA-4OHcinn was 97.8% efficient in protecting mild steel in saline solutions at neutral pH and prevented biofilm formation in marine environments.[18,19] Catubig and co-workers reported that a mixture of cetrimonium 4-hydroxycinnamate (Cet-4OHCin), with lanthanum 4-hydroxycinnamate (La-4OHCin), could considerably decrease the growth of bacteria strains implicated in microbially influenced corrosion (MIC) and confer a similar corrosion inhibition to that of La-4OHCin.[20]

Other studies revealed that the CTA-OHcinn forms micelles that are susceptible to changes in morphology according to concentration, environment pH, and the metal−electrolyte interface, which consequently affects the anticorrosive properties.[17,21,22] In addition, the nature of the cinnamate anion greatly affects the inhibition mechanism. It was shown that replacing the hydroxyl group of the anion with an ethoxy group changes the micellization of the inhibitor. In the latter case, the formation of elongated micelles was reported. The resulting salt, cetrimonium 4-ethoxy-cinnamate, offered greater protection than CTA-OHcinn and lower toxicity against zebrafish embryos.[21] It is expected that the increase of the hydrophobic alkyl chain length on the cinnamate anions decreases the inhibitor solubility and potentially increases their corrosion protection.[23,24]

Most of that work focused on neutral, chloride-contaminated aqueous solutions. Herein, the aim is to investigate the corrosion protection of carboxylate anions with different alkyl chain lengths (*trans*-4-hydroxycinnamate, *trans*-4-ethoxy-cinnamate, and *trans*-4-butoxy-cinnamate) linked to the CTA cation (Figure 1) in comparison with CTAB, in acid conditions of pH 1 and 2, which are of importance in various industrial applications, where a pH of 1 is around 5% HCl solution.[1] The effect of increasing chain length will likely affect the hydrophobicity, and the effect of this on the structure in solution and its subsequent protection are discussed.

The anticorrosive properties of the inhibitors in solution were investigated by electrochemical analysis. The use of waterborne coatings using materials is a way to reduce the environmental impact of coatings; thus, here, the inhibitors were blended with an acrylic polymeric binder obtained by dispersion polymerization in a reduced VOC system. The composite coatings were analyzed by electrochemical impedance spectroscopy (EIS) under neutral and acidic saline corrosive solutions. The behavior of these surfactant-like inhibitors was also investigated in solution using transmission electron microscopy (TEM) and NMR spectroscopy, together with molecular dynamics (MD) simulations (in the case of CTA-4BtOcinn), to investigate the nature of the micelles under low pH conditions.

METHODS

Materials and Specimen Preparation. The inhibitors are listed in Figure 1. The preparation method of these compounds was reported in earlier works.[17,21] For the coating studies, methyl methacrylate (MMA) and *n*-butyl acrylate (BA) (Quimidroga) were used as received. Methoxypolyethylene glycol methacrylate, 50% in aqueous solution (Visiomer MPEG 2005, Evonik), was used as an anionic emulsifier in the dispersion polymerization reactions. 2′-Azobis(2-methylbutyronitrile) (AMBN, Aldrich) was used as

https://doi.org/10.1021/acsomega.4c07098
ACS Omega 2025, 10, 18225−18237

a radical initiator. Distilled water and methanol (70 water:30 methanol) were used in the aqueous media in the reactions, and Milli-Q water was used for the electrochemical tests. The procedure for preparing the dispersion latexes was developed previously,[25] with a detailed description of the work reported here in the Supporting Information. Mild steel substrates were used for electrochemical tests of inhibitors in solution and for the formation of dispersion latex films.

For the immersion and electrochemical tests of inhibitors in solution, cylindrical coupons of AS1030 mild steel were embedded in epoxy resin, leaving an exposed circular area of 0.786 cm^2 (1 cm diameter). Before each experiment, the exposed areas were polished with 240, 600, and 1200 grit silicon carbide paper using a mechanical polisher with a continuous flow of distilled water. Then, the samples were dried with a nitrogen drying gun and placed in a silica gel desiccator for 1 h prior to the tests. Solutions of 0.01 M NaCl, with Milli-Q water, and 0.1 mM of each inhibitor were prepared as well as a control solution with no inhibitors. A solution of 0.1 mM CTAB and 0.01 M NaCl at pH 1 was also prepared for comparison purposes. This concentration corresponds to ppm values of 45, 48, 50, and 36 for CTA-OHcinn, CTA-MeOcinn, CTA-ButOcinn, and CTAB, respectively. To improve compound solubilities, the solutions were heated to 40 °C with a magnetic stirrer. After cooling, the pH of the solutions was adjusted to 2 or 1 with the addition of a diluted solution of HCl. Solutions were stored at room temperature and they remained clear, indicating that the inhibitors stayed in solution.

Immersion Tests, Optical, and Scanning Electron Microscopy (SEM) Analysis. Coupons were immersed in the solutions of inhibitors for 24 h and then gently rinsed with Milli-Q water, dried with a nitrogen drying gun, and placed in a silica gel desiccator. Optical images were taken using a Leica DMi8 microscope, and SEM images were performed using a JEOL IT300. Some immersion tests were also carried out for 4 days in order to compare the performance of the inhibitors for a longer period of time.

Potentiodynamic Polarization (PP) and Electrochemical Impedance Spectroscopy (EIS). Electrochemical measurements were performed at 25 °C using a low current channel of a BIO-LOGIC VMP3 potentiostat with EC Lab 11.27 software. A conventional three-electrode cell was used, composed of a saturated silver/silver chloride reference electrode in saturated KCl, a titanium mesh as the counter electrode, and AS1030 mild steel as the working electrode.

The open circuit voltage (OCV) was monitored for 47 min over the frequency range from 100 kHz to 10 mHz, followed by EIS at a scan rate of 0.167 mV/s with 6 points per decade and a sinusoidal amplitude of 10 mV. Impedance responses were monitored for 24 h, followed by a PP experiment. Separate PP experiments were also performed after 30 min of immersion, and all experiments were carried out in triplicate.

The corrosion current density (i_{corr}) and corrosion potential (E_{corr}) values were extracted from the PP curves by Tafel extrapolation. The linearity of the curves was found to be the highest over a range of 10−25 mV at both sides of E_{corr}. The value of i_{corr} corresponds to the point on the graph in which the linear extrapolations of the anodic and cathodic sections of the curves intersect. The inhibitor efficiency (IE) was calculated as shown in eq 1.

$$\mathrm{IE} = \frac{I_{\mathrm{corr\ control}} - I_{\mathrm{corr\ inhibited}}}{I_{\mathrm{corr\ control}}} \times 100 \quad (1)$$

Cryo-TEM Imaging of Micelles. Solutions of 1 mM cetrimonium cinnamate inhibitors in corrosive solutions of 0.01 M NaCl were prepared for cryo-TEM imaging. The solution was contained in a holder coated with a negatively charged carbon film. Copper grids (200 mesh) coated with a holey carbon film (Quantifoil R1.2/1.3) were placed in a Pelco glow discharge unit to render them hydrophilic. A sample volume of 3.5 μL was applied onto the grids, which were then blotted against two filter papers for 3 s at a blot force of −3 in a Vitrobot plunge freezer system (FEI). The resulting thin sample film was vitrified in a controlled environment vitrification system at 5 °C and 100% relative humidity by plunging the sample into liquid ethane, which was maintained at its melting point (−160 °C) with liquid nitrogen. The vitrified specimens were transferred to a Gatan 626 cryoholder and observed at an operating voltage of 120 kV in a Tecnai 12 Transmission Electron Microscope (FEI) at temperatures between −170 and −175 °C. Images were recorded with a Gatan Eagle high-resolution charge-coupled device (CCD) camera (4k × 4k) and digitized with the Tecnai Image Acquisition (TIA) program.

Preparation of Coated Steel Substrates and EIS of Coatings. After being polished to a 1200 grit finish, the steel substrates were cleaned with acetone and dried with compressed air before deposition of the dispersion latex with or without inhibitor. The coated samples were dried at room temperature for at least 1 day. The final thickness of the coatings was measured with a coating thickness gauge to ensure that the final film had an average thickness of 45−50 μm.

The properties of the coatings were evaluated (in triplicate) by electrochemical impedance spectroscopy (EIS) over 24 h using a low current channel of a BIO-LOGIC VMP3 potentiostat with EC Lab V11.26 software. The experiments were carried out at room temperature and open to air, with a cell composed of an Ag/AgCl reference electrode, AS1030 mild steel substrates as the working electrode, and a graphite rod counter electrode. The tests were carried out using an exposure area of 1.1 cm^2 and a corrosive solution of 0.005 M NaCl. The open circuit (OCV) was monitored for 47 min over the frequency range from 100 kHz to 10 mHz followed by EIS at a scan rate of 0.167 mV/s with 6 points per decade and a sinusoidal amplitude of 10 mV. This measurement was repeated hourly for 24 h.

Modeling Section. All-atom simulations were performed using the CHARMM force field.[26] Parameters for cetrimonium and 4-butoxy cinnamic acid were obtained using CGenFF.[27] The resulting charge distribution for cetrimonium and 4-butoxy cinnamic acid is shown in Figure S-1. All the systems were pre-equilibrated with an NVT and then an NpT ensemble for at least 20 ns prior to the MD production. An annealing process using the NVT ensemble was adopted to improve the dynamics, where the system was heated from 300 to 400 K and cooled from 400 to 300 K in the first 10 ns. The following 10 ns was run in an NpT ensemble at 300 K and 1 bar. The temperature and pressure were controlled by using a Nosé−Hoover thermostat and a Parrinello−Rahman barostat, respectively. This method is similar to that previously established for the cetrimonium system.[22]

https://doi.org/10.1021/acsomega.4c07098
ACS Omega 2025, 10, 18225−18237

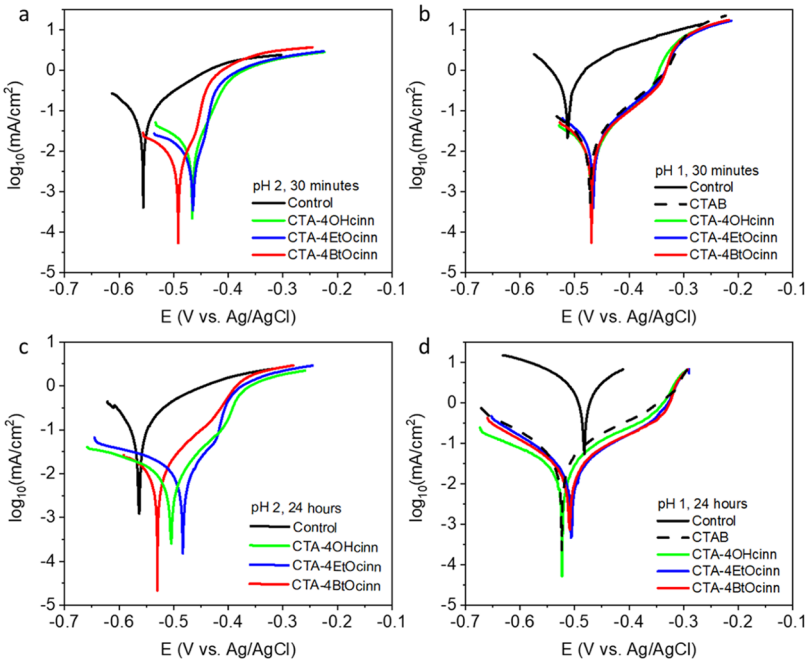

Figure 2. Representative polarization curves after immersion of mild steel in 0.01 M NaCl and 0.1 mM inhibitors solutions: (a) pH 2 after 30 min, (b) pH 1 after 30 min, (c) pH 2 after 24 h, and (d) pH 1 after 24 h.

Table 1. Corrosion Current Density (i_{corr}), Corrosion Potential (E_{corr}), Pitting Potential (E_{pit}), and Inhibitor Efficiency (IE) Extracted from the Polarization Curves Mild Steel Immersed Different Inhibitor Solutions

pH	sample	concentration (mM)	time (h)	i_{corr} (μA/cm^2)	E_{corr} (mV)	E_{pit} (mV)	IE (%)
2	control	0	0.5	21.6 ± 1.2	−560 ± 6.2		
		0	24	25.7 ± 3.3	−562.8 ± 7		
	CTA-OHcinn	0.1	0.5	5.4 ± 1.2	−461.3 ± 3.4		75.0
		0.1	24	1.9 ± 0.4	−504.6 ± 2.3	−364.5 ± 7.6	92.6
	CTA-EtOcinn	0.1	0.5	3.6 ± 0.7	−462.0 ± 3.5		83.3
		0.1	24	2.5 ± 0.4	−487.4 ± 5.8	−420.2 ± 3.3	90.3
	CTA-BtOcinn	0.1	0.5	2.6 ± 0.2	−491.6 ± 1.5	−460 ± 2.4	87.8
		0.1	24	3.3 ± 0.4	−529.9 ± 2.2	−425 ± 6	87.2
1	control	0	0.5	136.8 ± 20.7	−513.1 ± 2.7		
		0	24	329.7	−483		
	CTA-OHcinn	0.1	0.5	3.2 ± 0.7	−459.1 ± 12.6	−356.8 ± 2.9	97.6
		0.1	24	4.8 ± 0.9	−521.1 ± 3.6	−348.5 ± 8.4	98.5
	CTA-EtOcinn	0.1	0.5	6.0 ± 0.6	−469.3 ± 6.9	−341.7 ± 0.9	95.6
		0.1	24	4.3 ± 0.4	−501.5 ± 4.0	−336.3 ± 11.1	98.7
	CTA-BtOcinn	0.1	0.5	4.9 ± 1.6	−469.1 ± 6.1	−343.5 ± 12.3	96.4
		0.1	24	6.2 ± 2.1	−519.9 ± 13.5	−330.5 ± 6.4	98.1
	CTAB	0.1	0.5	7.6	−459.0	−332.9	94.4
		0.1	24	12.9	−521.0		96.1

For the coarse-grained model, the Martini force field with polarizable water was used.[28] Parameters for cetrimonium were taken from a previous study,[29] and since there is no literature reporting 4-butoxy cinnamic acid coarse-grained parameters, bottom-up parametrization was performed, beginning from its corresponding all-atom model. Bonded interactions were validated by comparing distance and angle distribution between the all-atom and coarse-grained models (Figure S-2). Additionally, nonbonded interactions were validated by comparing the energy profile of 4-butoxy cinnamic acid when it migrates from water to octanol for the all-atom and coarse-grained models (Figure S-3). Both models have similar partition energies of around −27 kJ/mol. A summary of the simulations with their respective composition and box dimensions is given in Table S-1. All the simulations were run in Gromacs 2020.3.[30]

RESULTS AND DISCUSSION

Electrochemical Analysis of Cetrimonium Cinnamate Cationic Surfactants as Free Inhibitors. Representative polarization curves obtained after 30 min and 24 h of immersion of mild steel in solutions of 0.01 M NaCl in pH 1 and pH 2 in the absence (control) and in the presence of free inhibitors are presented in Figure 2, and the data extracted from the Tafel extrapolation are shown in Table 1. A significant change in both anodic and cathodic currents can be seen, with a general shift in E_{corr} toward less negative values, suggesting a slightly larger effect on the anodic reaction. A

https://doi.org/10.1021/acsomega.4c07098
ACS Omega 2025, 10, 18225−18237

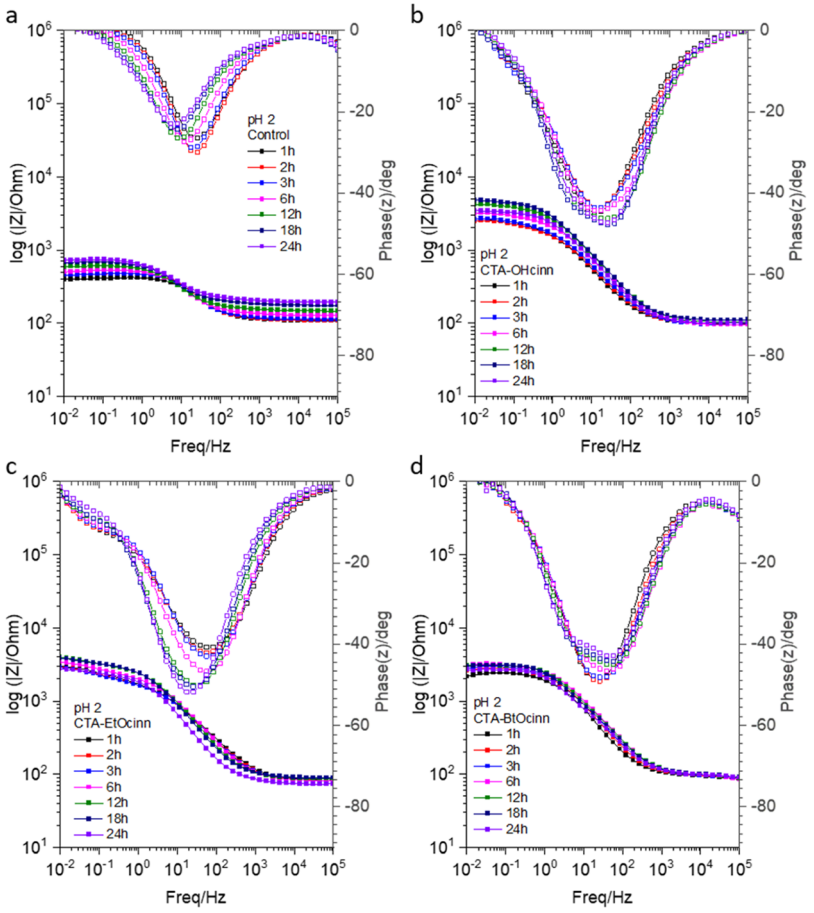

Figure 3. Bode plot and phase angle of inhibitors in solution at pH 2, (a) control, (b) CTA-OHcinn, (c) CTA-EtOcinn, and (d) CTA-BtOcinn.

reduction of corrosion current density (i_{corr}) is observed in all of the inhibitor-containing solutions after 30 min of immersion, when compared to the control, from 21.6 μA/cm^2 for control to 5.4 μA/cm^2 for CTA-4OHcinn, 3.6 μA/cm^2 for CTA-4MeOcinn, and 2.6 μA/cm^2 for CTA-4ButOcinn indicating that the inhibitors can suppress the process of dissolution of iron even at extreme acid conditions (Figure 2 and Table 1). Interestingly, comparing the corrosion current densities from pH 2 to 1, those of the control increase by almost an order of magnitude, while those of the inhibited solutions barely increase at all. Under these conditions, the results obtained for the solution of CTAB at pH 1 are larger than all the inhibitors, but not significantly, particularly after 30 min (Figure 2b and Table 1). After 24 h at pH 1, the differences increase, with i_{corr} for the CTAB being 12.9 μA/cm^2 compared to 4.8 μA/cm^2 for CTA-4OHcinn, 4.3 μA/cm^2 for CTA-4MeOcinn, and 6.2 μA/cm^2 for CTA-4ButOcinn. This suggests that there is some synergy between the carboxylate and the cetrimonium inhibitors after 24 h immersion.

After 24 h of immersion, E_{corr} for all inhibitors moves to more negative values, particularly at pH 1, which may be due to increased cathodic protection with time. The data clearly show consistent corrosion protection with time, with similar i_{corr} values at 30 min and 24 h, compared to the control, which increases in solutions, but particularly so at pH 1, with an increase from 137 to 330 μA/cm^2.

Bode plots of impedance and phase angles obtained from EIS measurements of the samples exposed to a corrosive solution without and with inhibitors at pH 2 and 1 are shown in Figures 3 and 4, respectively. The impedances of the samples with inhibitors are considerably higher ($10^{3.2}$−$10^{3.5}$ |Z| for pH 2 and $10^{3.1}$−$10^{3.2}$ for pH 1) than those observed for the control sample (maximum of $10^{2.8}$ |Z| for pH 2 and maximum of $10^{1.2}$ |Z| for pH 1), which confirms the corrosion protection given by these inhibitor compounds under harsh acidic conditions. The same is observed with the phase angles, being higher in the systems with inhibitors (maximum of approximately 50° at pH 2 and 70° at pH 1) than in the control systems (reaching a maximum of 30° at pH 2 and 20° at pH 1).

At pH 1, the highest phase angle is found in the solution of CTA-BtOcinn at 70° (Figure 4d) and the broader phase angle is found in the sample with CTA-OHcinn (Figure 4b), which can be an indication that this inhibitor is able to form a more stable film on the metal surface. The impedance obtained for the cetrimonium cinnamate surfactants at pH 1 (Figure 4a−d), in all cases, is higher ($10^{3.1}$−$10^{3.2}$ |Z|) than that obtained for the solution of CTAB ($10^{2.6}$−$10^{3.1}$ |Z|) (Figure 4e), confirming the increase of efficiency when the carboxylate anion is also present in the inhibitor compound. While the sample immersed in CTAB initially showed similar impedance values to the others, it was also the only one to significantly reduce, showing its lowest value of $10^{2.6}$ after 24 h, indicating that it does not attach to the surface as strongly.

Optical and SEM Analysis of Samples Immersed in Solutions of Inhibitors. Optical and SEM images of the coupons after immersion for 24 h in the solutions are presented in Figure 5. The control sample immersed in a saline

https://doi.org/10.1021/acsomega.4c07098
ACS Omega 2025, 10, 18225−18237

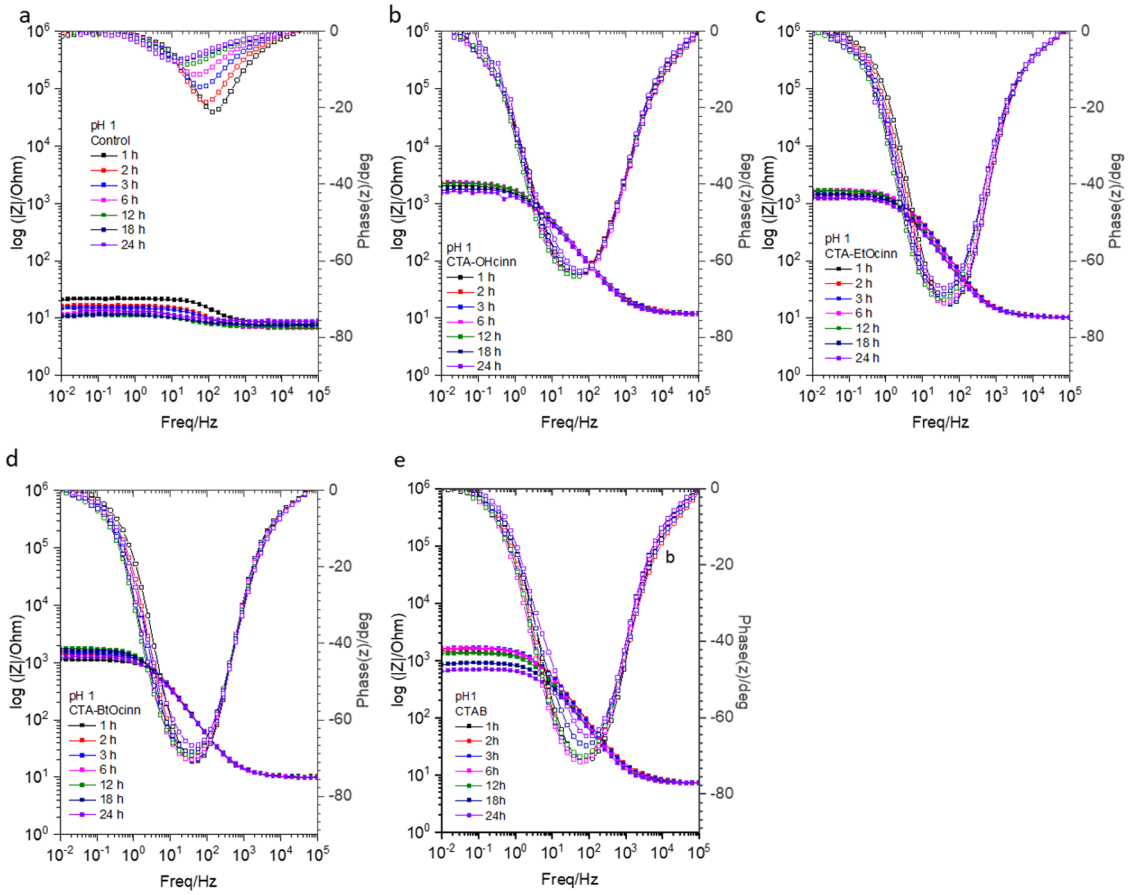

Figure 4. Bode plot and phase angle of inhibitors in solution at pH 1, (a) control, (b) CTA-OHcinn, (c) CTA-EtOcinn, (d) CTA-BtOcinn, and (e) CTAB.

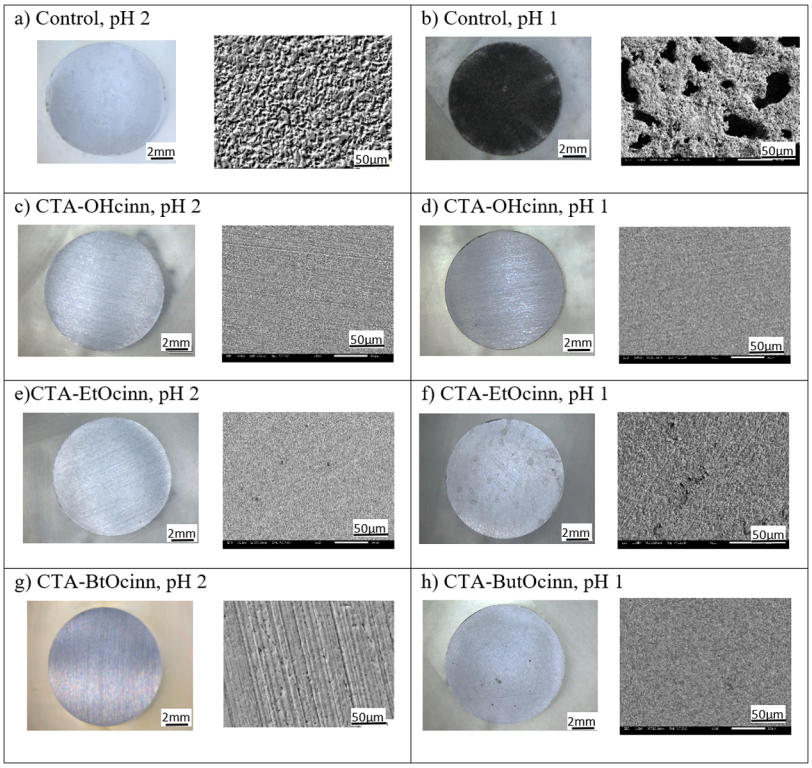

Figure 5. Optical images (left) and SEM images 5000× (right) of samples after 24 h of immersion in corrosive solutions with 0.1 mM of inhibitor.

https://doi.org/10.1021/acsomega.4c07098
ACS Omega 2025, 10, 18225−18237

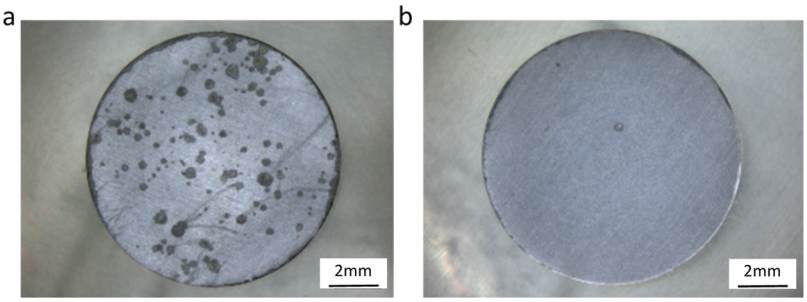

Figure 6. Optical images of samples immersed in a corrosive solution of 0.1 mM of inhibitor at pH 1 for 4 days: (a) CTAB and (b) CTA-OHcinn.

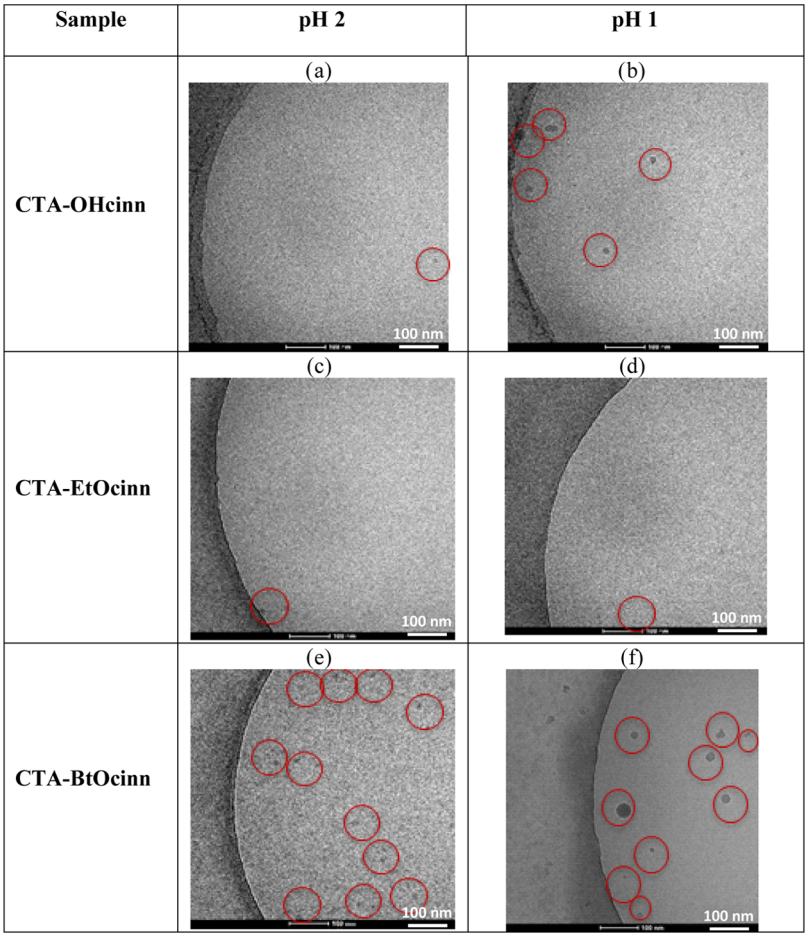

Figure 7. Cryo-TEM image solutions of 0.1 mM cetrimonium cinnamate proposed inhibitors with 0.1 M NaCl, at pH 2: CTA-OHcinn (a), CTA-EtOcinn (c), and CTA-BtOcinn (e) and at pH 1: CTA-OHcinn (b), CTA-EtOcinn, and (d) CTA-BtOcinn (f).

solution of pH 1 (Figure 5b) is significantly more corroded than the one immersed at pH 2 (Figure 5a), which shows the corrosive capacity of the solution at lower pH as indicated by the significant increase in i_{corr}. At pH 2, a significant amount of pitting is observed on the sample surface, while at pH 1 part of the material seems to be dissolved forming voids and holes on the surface. However, the compounds immersed in the inhibitor solutions showed only mild corrosion. The anticorrosive protection given by the inhibitors to the mild steel at pH 1 is highly efficient, especially when compared to the control sample at the same pH, consistent with the polarization and EIS results presented above (Figures 3 and 4).

To determine whether the slightly lower impedances seen for CTAB than the cetrimonium cinnamates indicate less protection from corrosion, the efficiency of the two surfactants was compared by immersing coupons for 4 days in solutions of 0.1 mM CTAB and CTA-OHcinn at pH 1 (Figure 6). The surface of the sample immersed in the solution of CTAB was covered with stains, showing visible signs of localized corrosion, while in contrast only mild signs of corrosion were seen for the steel surface immersed in the acidic solution containing CTA-OHcinn. This is consistent with the reduction in impedance seen after 24 h for CTAB and confirms the superior inhibition efficiency of cetrimonium cinnamate compounds compared to CTAB alone.

Cryo-TEM Imaging of Micelles. The formation of wormlike entangled micelles from CTA-OHcinn and CTA-EtOcinn was previously reported at neutral pH values and

https://doi.org/10.1021/acsomega.4c07098
ACS Omega 2025, 10, 18225−18237

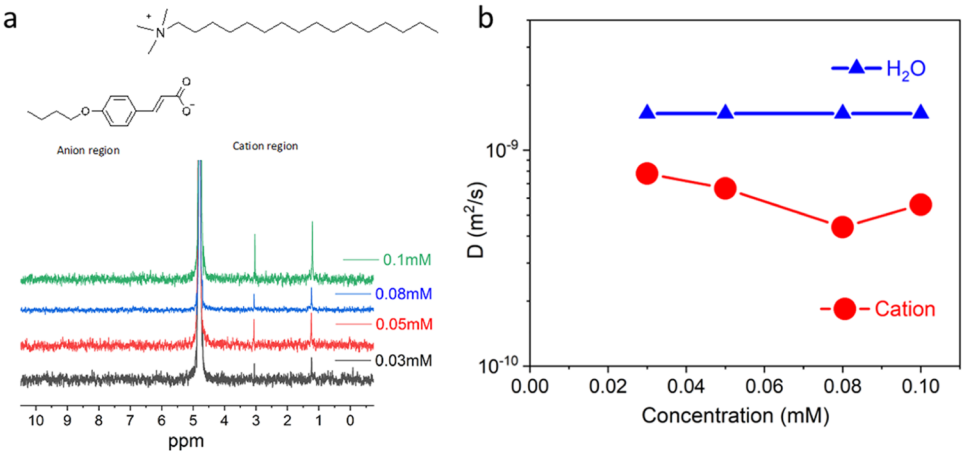

Figure 8. (a) ^{1}H NMR spectra of CTA-BtOcinn as a function of concentration and (b) ^{1}H diffusion of CTA-BtOcinn as a function of concentration; experiment setup: 0.01 M NaCl, 20 °C, pH 2.

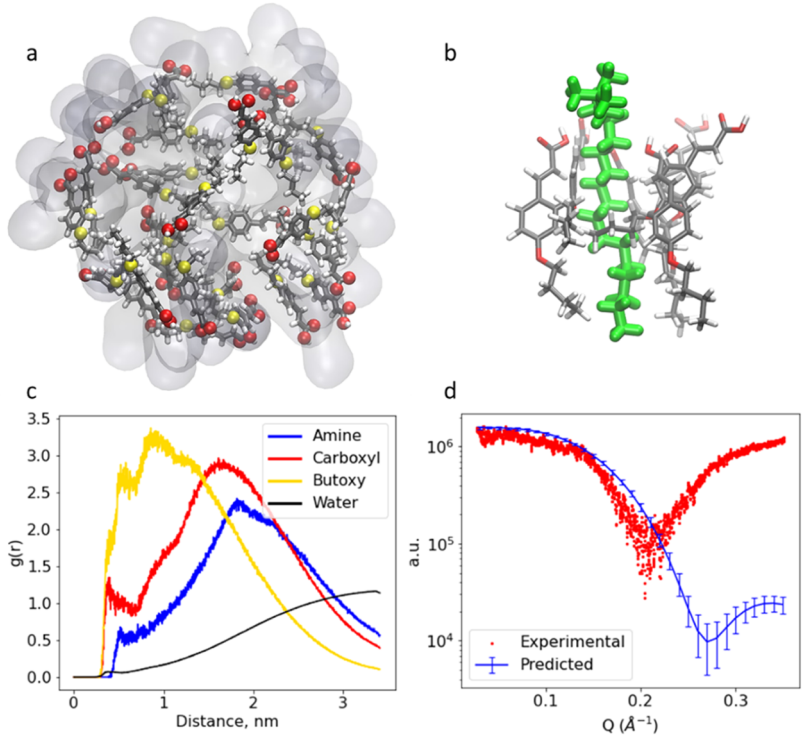

Figure 9. (a) Simulation snapshot of the inhibitor micelle. Cetrimonium cations are hidden, and their shapes are represented by the gray transparent color. The carboxyl and butoxy groups of 4-butoxy cinnamic acid are red and yellow, respectively. (b) Tight conformation of a cetrimonium cation with five 4-butoxy cinnamic acid molecules. (c) Radial distribution functions taking as a reference the cetrimonium last carbon tail for different molecular groups. (d) Predicted and experimental small-angle X-ray scattering (SAXS) data.

evidenced by both TEM and MD simulations.[22] Therefore, here, we also examined the micellar formation at low pH values of pH 1 and 2 using cryo-TEM imaging of solutions containing 0.1 mM of each cetrimonium cinnamate. The obtained cryo-TEM images are presented in Figure 7, and the observed micelles are labeled with red circles for better visualization. Spherical micelles are observed in all of the inhibitors at pH 1 and pH 2.

It is known that the shape of the formed micelles as well as the efficiency of the inhibitor may change due to temperature, inhibitor concentration, solution pH, and changes to the alkyl tail on the cinnamate anion.[17,22] It seems that larger micelles are present in the solution at pH 1 than in pH 2 (Figure 7), with the biggest micelles formed in the solution of CTA-4BtOcinn (Figure 7f) at pH 1, which may be due to the longer alkyl tail of the anion.

NMR Measurements. To further understand the corrosion inhibition observed with the CTA-BtOcinn, the possible micellar formation of this compound was explored by studying the diffusion coefficients for each component in aqueous solution as a function of concentration at pH 2 using pulsed-field gradient nuclear magnetic resonance (PFG-NMR) spectroscopy (Figure 8).

Figure 8a shows representative NMR spectra, from which the cation peaks are clearly seen; however, no anion peaks appear, and thus, anion diffusion could not be determined. The

https://doi.org/10.1021/acsomega.4c07098
ACS Omega 2025, 10, 18225−18237

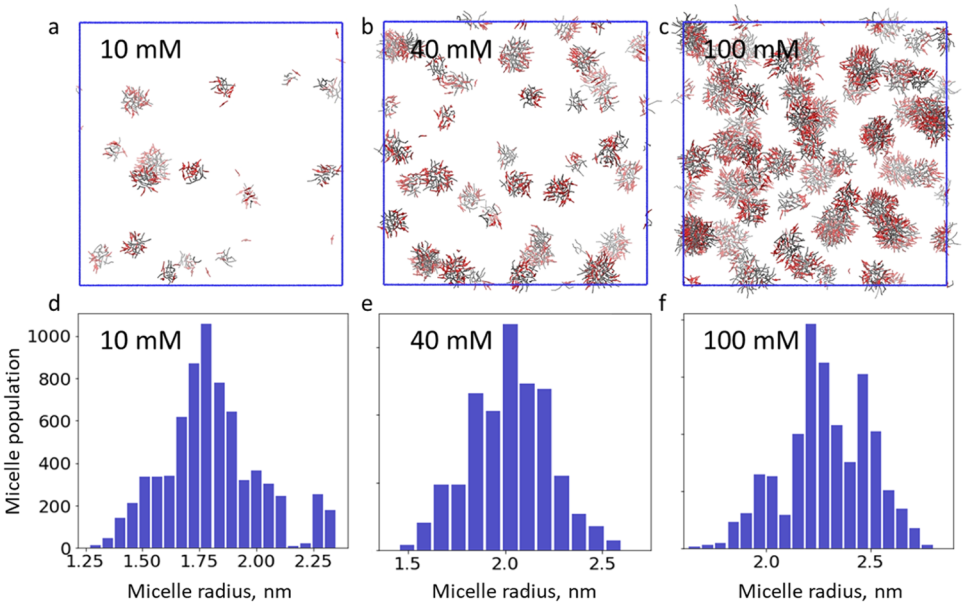

Figure 10. (a–c) Coarse-grained simulation snapshots of cetrimonium and 4-butoxy cinnamic acid micelles colored in gray and red, respectively, at different concentrations. (d–f) Size distribution of micelles at different concentrations.

peak at 4.8 ppm corresponds to D_2O solvent; the peak around 3 ppm corresponds to H in the three methyl groups attached to N; the peak around 1.2 ppm corresponds to H in the methylene groups from the 3rd to the 15th C starting from N. We postulate that the absence of the anion peaks may be because the BtOcinn anions are encapsulated within the CTA cation micelles and are effectively immobilized and cannot diffuse fast enough to be seen in the pulsed field gradient. This indicates significant anion entrapment and its strong interactions (Coulombic and cation-π bonding) within the micellar shell.[30,31] On the other hand, it is likely that cations are exchanging with the micelle and the solution and hence on average are more diffusive and have narrower peaks. Figure 8b shows the NMR diffusion data of CTA-BtOcinn as a function of the concentration at room temperature. Given the absence of the anion peaks in the spectra, only the cation and water diffusion could be determined. The diffusion coefficient of the CTA cation is significantly lower than the water solvent diffusion, which suggests the presence of micelles. The continuous decrease in diffusion up to 0.08 mM suggests micellar growth, with solvent diffusion eventually remaining constant.[32,33] In previous works with CTA-OHcinn and CTA-EtOcinn at neutral pH, the NMR data showed significant concentration dependence at pH 7 with the diffusion for the CTA cation decreasing from 4×10^{-10} cm^2/s at 0.1 mM to 2×10^{-11} cm^2/s at 1 mM concentration.[17,21] It was suggested that an aromatic carboxylate anion can become incorporated within the CTA surfactant cation micellar structure, and this incorporation will affect the molecular packing factor that determines micelle shape and sizes. In the previously reported case, the micelle changed from spherical to cylindrical or wormlike shape as the concentration increased. MD simulations for the CTA-EtOcinn clearly showed wormlike micelles forming in this case at pH 7, which was consistent with the cryo-TEM data reported.

Here, we were unable to dissolve a high concentration of the CTA-4BtOCin at low pH, and so the diffusion is only measured up to 0.1 mM concentration where a value of 6×10^{-10} cm^2/s was measured, slightly higher than for the previous cases. The absence altogether of the anion NMR peaks and diffusion suggests that the micellar structure is different from the wormlike micellar structure seen in our previous work, consistent also with the TEM images shown above.

MD Simulations. To further investigate the structure of the inhibitors in solution, MD simulations were conducted. The all-atom model shows the self-assembly of cetrimonium and 4-butoxy cinnamic acid, forming a spherical aggregate (Figure 9a). On average, 4-butoxy cinnamic acid follows a certain orientation within the micelle. The carboxyl groups from the acid are closer to the cetrimonium amine groups on the micelle surface, while the butoxy groups are closer to the cetrimonium micelle core (Figure 9c). A similar orientation was reported in modeling studies of other cinnamate derivatives.[21,22,29] Such a conformation of 4-butoxy cinnamic acid in the micelle can be attributed to the localized negative charge of the carboxyl groups (Figure S-1), which coordinate with the positive amine groups from cetrimonium on the micelle surface. Conversely, the butoxy group of the acid prefers to stay within the micelle due to van der Waals interactions with the cetrimonium tail. Previous studies on similar micelles have shown that such an arrangement can result in the amine group being attracted to the metal surface, following which the carboxylate on the cinnamate forms hydrogen bonds with the surface.[22] Since CTAB does not have any cinnamate present, it relies only on the interaction of the amine group with the surface, thus explaining why it does not protect the surface as well.

The tight packing of the 4-butoxy cinnamic acid within the micelle (Figure 9b) is consistent with the NMR analysis of cetrimonium 4-butoxy-cinnamate, where the diffusivity of the surfactant and aromatic overlaps. Following that, the SAXS curve was predicted from the simulation trajectory using the WAXSiS server[34] and compared with experimental data (Figure 9d). In both cases, a similar shape is obtained, consistent with a suspension of ellipsoidal aggregates.[35] However, the minimum point of the experimental curve is lower than the predicted one, which indicates that the model underestimates the micelle size.

https://doi.org/10.1021/acsomega.4c07098
ACS Omega 2025, 10, 18225−18237

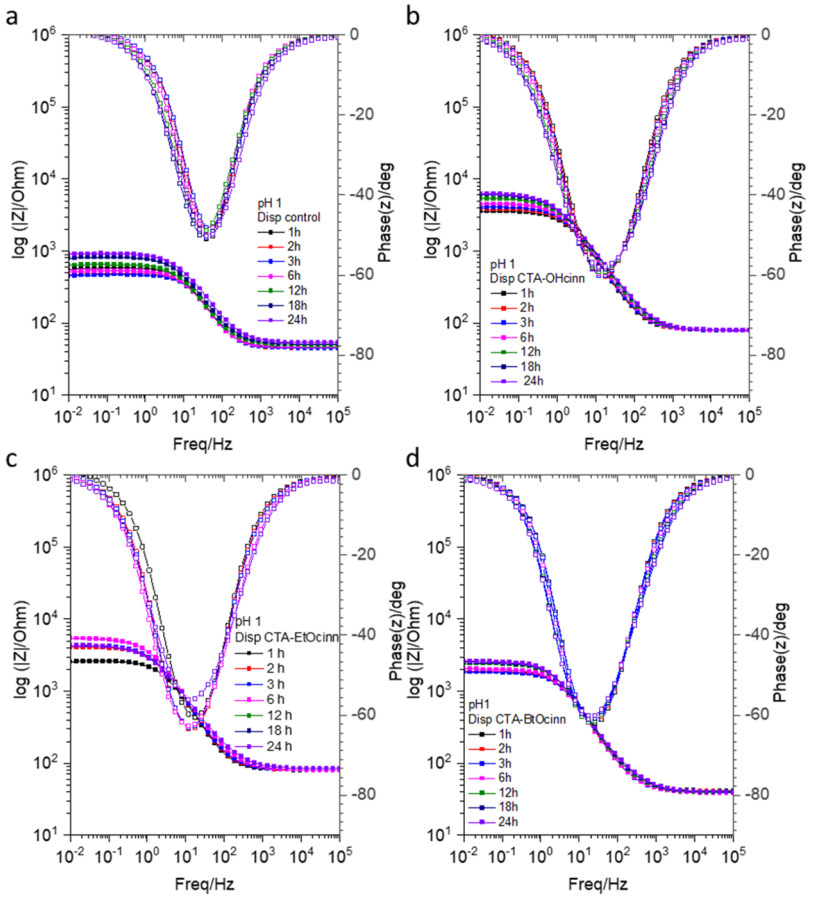

Figure 11. Bode plot and phase angle of coatings with inhibitors blended tested in a corrosive solution of 0.005 M NaCl and pH 1: (a) control, (b) CTA-OHcinn, (c) CTA-EtOcinn, and (d) CTA-BtOcinn.

Table 2. Fitting Results for Dispersion Coatings after 24 h of Experiment at pH 1, with Inhibitors Blended

sample	R_s (Ω)	C_{coat} ($\mu F/s^{n_{coat}}$)	n_{coat}	R_{pore} (Ω)	C_{dl} ($\mu F/s^{n_{dl}}$)	n_{dl}	R_{ct} (Ω)	χ^2/|Z|
Dp_control	53.07	24.42	0.8250	0.1319	24.83	0.8250	870	0.0055
Dp_CTA-OHcinn	77.10	40.36	0.7739	5828	11.17	0.9751	446.3	0.0069
Dp_CTA-EtOcinn	83.53	45.81	0.7830	3102	5.657	0.3000	1172	0.0064
Dp_CTA-BtOcinn	46.38	42.6	0.8529	1315	10.75	0.5442	1245	0.3381

Additionally, coarse-grained modeling was used to study the effect of the inhibitor concentration on the micelle formation. At all inhibitor concentrations, 10, 40, and 100 mM, spherical micelles are formed, consistent with cryo-TEM imaging (Figure 10a–c). It is also noticed that the micelle average radius increases from around 1.75 to 2.3 nm with inhibitor concentration (Figure 10c–e). The increase in micelle radius with surfactant concentration was reported for dodecyl trimethylammonium chloride (DTAC) using dynamic light scattering.[36] Such an increase in micelle size can be related to enhanced corrosion protection at higher inhibitor concentrations due to better surface coverage and a thicker layer,[17,18] as demonstrated experimentally.

Corrosion Protection of Cetrimonium Cinnamate Inhibitors Blended in Polymer Coatings. To assess the inhibitor performance in latex-based polymeric coatings, the different cetrimonium cinnamate inhibitors were blended into acrylic binders produced by dispersion polymerization. The protection provided by the control film and by the films with the inhibitor blended, after coated on steel, was analyzed by EIS in neutral pH 7 (Figure S-4) and in acid solutions (Figure 11).

The Bode spectra of the control coatings in neutral pH (Figure S-4) are characteristic of soft coatings that allow diffusion of water, and it has no phase angle peaks at high frequencies that are normally associated with a barrier coating.[37] Therefore, the control-dispersion coating offers no significant anticorrosive protection to the bare steel substrate. Higher impedances and phase angles are observed in the first hour of analysis of the coatings with CTA-EtOcinn and CTA-BtOcinn (Figure S-4) due to the anticorrosive properties of the inhibitors in the films. Nevertheless, the inhibitors are not able to maintain protection to the system at longer times. Since the coating is highly permeable, the inhibitor may be washed out of the coating (Figure S-4).

At pH 1, due to the higher concentration of ions in the system, impedance values in the higher frequency range of the Bode plot of the immersed samples are lower (Figure 11) when compared to the data obtained under neutral conditions. Higher impedances are seen for the coatings with inhibitor (Figure 11b–d) when compared to the control (Figure 11a).

https://doi.org/10.1021/acsomega.4c07098
ACS Omega 2025, 10, 18225−18237

Contrary to what was seen in the system immersed at neutral pH, the inhibitors here are able to retain higher impedance and phase angle values for the duration of the 24 h experiment, suggesting some potential for these compounds to be released in acidic pH to protect the underlying metal.

The equivalent circuit (EC) typically employed in the representation of coatings (Figure S-5) was used to fit the EIS spectra of the control coating, and coating with the inhibitors was blended at pH 1, after 24 h of the experiment.[3,37] R_s represents the solution resistance, C_{coat} is the coating capacitance, R_{pore} is the resistance in the pores of the coating, C_{dl} represents the double-layer capacitance at the interface, and R_{ct} is the charge transfer resistance at the interface. The fitting results are listed in Table 2.

The fitting results obtained for the experiments at pH 1 show that for the coatings with inhibitors blended within them higher values of C_{coat} compared to the control are measured. Typically, a higher capacitance is related to poor inhibition protection. However, the overall resistance is still higher compared to the control test since the pore and charge transfer resistances are considerably high in the inhibited samples. The highest value is found in the coating with CTA-OHcinn. A lower value of C_{dl} is observed in the coatings with inhibitors, which is frequently associated with less corroded surfaces,[38] while the values of R_{pore} and R_{ct} increase with the addition of the inhibitors. These increases in R_{pore} and R_{ct} indicate that the inhibitors are actively improving the protection by both blocking pores and increasing the resistance at the coating/metal interface, indicating that the inhibitors can provide further protection to the surface.

CONCLUSIONS

With increasing restrictions on the chemicals that can be used as corrosion inhibitors, the discovery of safe and effective compounds that are effective for acidic conditions is of growing importance. In this work, a range of three cetrimonium cinnamate cationic surfactants (CTA-OHcinn, CTA-EtOcinn, and CTA-BtOcinn) were studied as inhibitors in solution, and all demonstrated an inhibition efficiency over 98% at pH 1. Longer-term immersion tests confirmed that the cetrimonium cinnamate CTA-OHcinn showed significantly less corrosion product than the halide anion containing the cinnamate CTAB.

A mechanistic study of the CTA-BtOcinn was undertaken using cryo-TEM, NMR, and MD simulations. Unlike our previous works, these studies indicated that CTA-BtOcinn only formed spherical micelles in the solutions tested. The PFG-NMR data are consistent with the observations from cryo-TEM imaging, which showed small spherical micelles with an average diameter of 5 nm. Furthermore, MD simulations illustrate the spherical micellar configuration and aggregation at the molecular level. In acidic solutions (e.g., at pH 1 or 2), the carboxylate is likely protonated, which impacts the micellar behavior in solution. Additionally, the longer alkyl chain on the BtOcinn anion increases the hydrophobicity, thus reducing the solubility. These factors likely result in only spherical micelles forming; however, they were able to form a highly effective protective film on the surface. As reported in our previous work,[17,22] it is envisaged that the entrapped anions are delivered to the metal surface via the micelles, where the carboxyl group attaches to the surface, forming a protective barrier on the steel surface and offering excellent corrosion protection under acidic conditions. The bonding of the carboxylate to the surface likely explains why CTA-OHcinn showed better performance than CTAB in the 4 day immersion at pH 1.

Preliminary results obtained from EIS tests of films formed from the blend of those cetrimonium cinnamate inhibitors into dispersion coatings in corrosive media of pH 7 and 1 strongly suggest that the studied cetrimonium cinnamates are functional for application as paint additives, being especially efficient at lower pHs.

ASSOCIATED CONTENT

Data Availability Statement

The raw/processed data required to reproduce these findings cannot be shared at this time due to technical or time limitations.

Supporting Information

The Supporting Information is available free of charge at https://pubs.acs.org/doi/10.1021/acsomega.4c07098.

> The waterborne latex polymerization, background information for the MD simulations, an equivalent circuit for the coatings at pH 1, and Bode plots for the coatings tested at pH 7 (PDF)

AUTHOR INFORMATION

Corresponding Authors

Maria Paulis − *POLYMAT, Kimika Fakultatea, Kimika Aplikatua Saila, University of the Basque Country UPV/EHU, Donostia-San Sebastián 20018, Spain;* orcid.org/0000-0002-7000-1231; Email: maria.paulis@ehu.eus

Anthony E. Somers − *Institute for Frontier Materials, Deakin University, Burwood, Victoria 3125, Australia;* orcid.org/0000-0002-0220-2904; Email: asomers@deakin.edu.au

Authors

Diulia Quites Rodrigues − *POLYMAT, Kimika Fakultatea, Kimika Aplikatua Saila, University of the Basque Country UPV/EHU, Donostia-San Sebastián 20018, Spain*

Mahdi Ghorbani − *Institute for Frontier Materials, Deakin University, Burwood, Victoria 3125, Australia;* orcid.org/0000-0002-4731-6526

Jhonatan Soto Puelles − *Institute for Frontier Materials, Deakin University, Burwood, Victoria 3125, Australia;* orcid.org/0000-0002-4120-0979

Simon Crawford − *Ramaciotti Centre for Cryo Electron Microscopy, Monash University, Clayton, Victoria 3800, Australia*

Maria Forsyth − *Institute for Frontier Materials, Deakin University, Burwood, Victoria 3125, Australia;* orcid.org/0000-0002-4273-8105

Complete contact information is available at: https://pubs.acs.org/10.1021/acsomega.4c07098

Notes

The authors declare no competing financial interest.

ACKNOWLEDGMENTS

M.G., J.S.P., M.F., and A.E.S. would like to thank the Australian Research Council for funding through DP180101465.

REFERENCES

(1) Finšgar, M.; Jackson, J. Application of corrosion inhibitors for steels in acidic media for the oil and gas industry: A review. *Corros. Sci.* **2014**, *86*, 17−41.

(2) Kaur, J.; Daksh, N.; Saxena, A. Corrosion Inhibition Applications of Natural and Eco-Friendly Corrosion Inhibitors on Steel in the Acidic Environment: An Overview. *Arabian J. Sci. Eng.* **2022**, *47*, 57−74.

(3) Peng, Y.; Hughes, A. E.; Deacon, G. B.; Junk, P. C.; Hinton, B. R. W.; Forsyth, M.; Mardel, J. I.; Somers, A. E. A study of rare-earth 3-(4-methylbenzoyl)-propanoate compounds as corrosion inhibitors for AS1020 mild steel in NaCl solutions. *Corros. Sci.* **2018**, *145*, 199−211.

(4) Chong, A. L.; Mardel, J. I.; MacFarlane, D. R.; Forsyth, M.; Somers, A. E. Synergistic Corrosion Inhibition of Mild Steel in Aqueous Chloride Solutions by an Imidazolinium Carboxylate Salt. *ACS Sustainable Chem. Eng.* **2016**, *4*, 1746−1755.

(5) Little, B. J.; Blackwood, D. J.; Hinks, J.; Lauro, F. M.; Marsili, E.; Okamoto, A.; Rice, S. A.; Wade, S. A.; Flemming, H. C. Microbially influenced corrosion—Any progress? *Corros. Sci.* **2020**, *170*, No. 108641.

(6) Lyon, S. B.; Bingham, R.; Mills, D. J. Advances in corrosion protection by organic coatings: What we know and what we would like to know. *Prog. Org. Coat.* **2017**, *102*, 2−7.

(7) Somers, A. E.; Deacon, G. B.; Hinton, B. R. W.; MacFarlane, D. R.; Junk, P. C.; Tan, M. Y. J.; Forsyth, M. Recent developments in environment-friendly corrosion inhibitors for mild steel. *J. Indian Inst. Sci.* **2016**, *96*, 285−292.

(8) Blin, F.; Leary, S. G.; Wilson, K.; Deacon, G. B.; Junk, P. C.; Forsyth, M. Corrosion Mitigation of Mild Steel by New Rare Earth Cinnamate Compounds. *J. Appl. Electrochem.* **2004**, *34*, 591−599.

(9) Forsyth, M.; Seter, M.; Hinton, B.; Deacon, G.; Junk, P. New 'Green' Corrosion Inhibitors Based on Rare Earth Compounds. *Aust. J. Chem.* **2011**, *64*, 812−819.

(10) Deacon, G. B.; Junk, P. C.; Lee, W. W.; Forsyth, M.; Wang, J. Rare earth 3-(4′-hydroxyphenyl)propionate complexes. *New J. Chem.* **2015**, *39*, 7688−7695.

(11) Seter, M.; Hinton, B.; Forsyth, M. Understanding Speciation of Lanthanum 4-Hydroxy Cinnamate and its Impact on the Corrosion Inhibition Mechanism for AS1020 Steel. *J. Electrochem. Soc.* **2012**, *159*, C181.

(12) Bai, Y.; Zhang, J.; Dong, S.; Li, J.; Zhang, R.; Pu, C.; Chen, Gang. Effect of anion on the corrosion inhibition of cationic surfactants and a mechanism study. *Desalin. Water Treat.* **2020**, *188*, 130−139.

(13) Soror, T. Y.; El-Zady, M. A. Effect of cetyl trimethyl ammonium bromide on the corrosion of carbon steel in acids. *Mater. Chem. Phys.* **2003**, *77*, 697−703.

(14) Fouda, A. S.; Migahed, M. A.; Atia, A. A.; Mousa, I. M. Corrosion Inhibition and Adsorption Behavior of Some Cationic Surfactants on Carbon Steel in Hydrochloric Acid Solution. *J. Bio TriboCorros.* **2016**, *2*, No. 22.

(15) Yan, H.; Han, Z.; Li, K.; Li, G.; Wei, X. Molecular dynamics simulation of the pH induced structural transitions in CTAB/NaSal solution. *Langmuir* **2018**, *34* (1), 351−358.

(16) Gopi, D.; Govindaraju, K. M.; Manimozhi, S.; Ramesh, S.; Rajeswari, S. Inhibitors with biocidal functionalities to mitigate corrosion on mild steel in natural aqueous environment. *J. Appl. Electrochem.* **2007**, *37*, 681−689.

(17) Ghorbani, M.; Soto Puelles, J.; Forsyth, M.; Catubig, R. A.; Ackland, L.; Machuca, L.; Terryn, H.; Somers, A. E. Corrosion Inhibition of Mild Steel by Cetrimonium trans-4-Hydroxy Cinnamate: Entrapment and Delivery of the Anion Inhibitor through Speciation and Micellar Formation. *J. Phys. Chem. Lett.* **2020**, *11*, 9886−9892.

(18) Soto Puelles, J.; Ghorbani, M.; Yunis, R.; Machuca, L. L.; Terryn, H.; Forsyth, M.; Somers, A. E. Electrochemical and Surface Characterization Study on the Corrosion Inhibition of Mild Steel 1030 by the Cationic Surfactant Cetrimonium Trans-4-hydroxy-cinnamate. *ACS Omega* **2021**, *6*, 1941−1952.

(19) Tuck, B.; Watkin, E.; Forsyth, M.; Somers, A.; Ghorbani, M.; Machuca, L. L. Evaluation of a novel, multi-functional inhibitor compound for prevention of biofilm formation on carbon steel in marine environments. *Sci. Rep.* **2021**, *11*, No. 15697.

(20) Catubig, R. A.; Michalczyk, A.; Neil, W. C.; McAdam, G.; Forsyth, J.; Ghorbani, M.; Yunis, R.; Ackland, M. L.; Forsyth, M.; Somers, A. E. Inhibitor mixture for reducing bacteria growth and corrosion on marine steel. *Aust. J. Chem.* **2022**, *75*, 619−630.

(21) Ghorbani, M.; Soto Puelles, J.; Forsyth, M.; Zhu, H.; Crawford, S.; Chen, F.; Cáceres-Vélez, P. R.; Jusuf, P. R.; Somers, A. Engineering Advanced Environmentally Friendly Corrosion Inhibitors, Their Mechanisms, and Biological Effects in Live Zebrafish Embryos. *ACS Sustainable Chem. Eng.* **2022**, *10*, 2960−2970.

(22) Soto Puelles, J.; Ghorbani, M.; Crawford, S.; Ackland, L.; Chen, F.; Somers, A. E.; Forsyth, M. Modelling cetrimonium micelles as 4-OH cinnamate carriers targeting a hydrated iron oxide surface. *J. Colloid Interface Sci.* **2022**, *610*, 785.

(23) Ali, S. A.; El-Shareef, A. M.; Al-Ghamdi, R. F.; Saeed, M. T. The isoxazolidines: the effects of steric factor and hydrophobic chain length on the corrosion inhibition of mild steel in acidic medium. *Corros. Sci.* **2005**, *47*, 2659−2678.

(24) Milošev, I.; Bakarič, T.; Zanna, S.; Seyeux, A.; Rodič, P.; Poberžnik, M.; Chiter, F.; Cornette, P.; Costa, D.; Kokalj, A.; Marcus, P. Electrochemical, Surface-Analytical, and Computational DFT Study of Alkaline Etched Aluminum Modified by Carboxylic Acids for Corrosion Protection and Hydrophobicity. *J. Electrochem. Soc.* **2019**, *166*, C3131.

(25) Quites, D.; Leiza, J. R.; Mantione, D.; Somers, A. E.; Forsyth, M.; Paulis, M. Incorporation of a Coumarate Based Corrosion Inhibitor in Waterborne Polymeric Binders for Corrosion Protection Applications. *Macromol. Mater. Eng.* **2022**, *307* (2022), No. 2100772.

(26) Vanommeslaeghe, K.; Hatcher, E.; Acharya, C.; Kundu, S.; Zhong, S.; Shim, J.; Darian, E.; Guvench, O.; Lopes, P.; Vorobyov, I.; Mackerell, A. D. CHARMM general force field: A force field for drug-like molecules compatible with the CHARMM all-atom additive biological force fields. *J. Comput. Chem.* **2010**, *31*, 671−690.

(27) Vanommeslaeghe, K.; Raman, E. P.; MacKerell, A. D., Jr Automation of the CHARMM General Force Field (CGenFF) II: assignment of bonded parameters and partial atomic charges. *J. Chem. Inf. Model.* **2012**, *52*, 3155−3168.

(28) Yesylevskyy, S. O.; Schäfer, L. V.; Sengupta, D.; Marrink, S. J. Polarizable water model for the coarse-grained MARTINI force field. *PLoS Comput. Biol.* **2010**, *6*, No. e1000810.

(29) Puelles, J. S.; Ghorbani, M.; Tuck, B.; Machuca, L. L.; Ackland, M. L.; Chen, F.; Somers, A. E.; Forsyth, M. Effect of cetrimonium carrier micelles on bacterial membranes and extracellular DNA, an in silico study. *Sci. Rep.* **2023**, *13*, No. 8041.

(30) Van Der Spoel, D.; Lindahl, E.; Hess, B.; Groenhof, G.; Mark, A. E.; Berendsen, H. J. C. GROMACS: fast, flexible, and free. *J. Comput. Chem.* **2005**, *26*, 1701−1718.

(31) Fleming, B. D.; Biggs, S.; Wanless, E. J. Slow Organization of Cationic Surfactant Adsorbed to Silica from Solutions Far below the CMC. *J. Phys. Chem. B* **2001**, *105*, 9537−9540.

(32) Zhang, J.-z.; Xie, L.; Chai, S.-g.; Zou, Q.-c. Interaction in Binary Mixtures of Gemini Surfactant G12−6-12 and CTAB by NMR. *Chin. J. Chem. Phys.* **2014**, *27*, 307−314.

(33) Senra, T. D. A.; Khoukh, A.; Desbrières, J. Interactions between quaternized chitosan and surfactant studied by diffusion NMR and conductivity. *Carbohydr. Polym.* **2017**, *156*, 182−192.

(34) Knight, C. J.; Hub, J. S. WAXSiS: a web server for the calculation of SAXS/WAXS curves based on explicit-solvent molecular dynamics. *Nucleic Acids Res.* **2015**, *43*, W225−W230.

(35) Ivanović, M. T.; Hermann, M. R.; Wójcik, M.; Pérez, J.; Hub, J. S. SAXS Curves of Detergent Micelles: Effects of Asymmetry, Shape Fluctuations, Disorder, and Atomic Details. *bioRxiv* **2019**, No. 815266.

(36) Ogino, K.; Kubota, T.; Uchiyama, H.; Abe, M. Micelle formation and micellar size by a light scattering technique. *J. Jpn. Oil Chem. Soc.* **1988**, *37*, 588−591.

https://doi.org/10.1021/acsomega.4c07098
ACS Omega 2025, 10, 18225−18237

(37) Murray, J. N. Electrochemical test methods for evaluating organic coatings on metals: an update. *Prog. Org. Coat.* **1997**, *31*, 375−391.
(38) Loveday, D.; Peterson, P.; Rodgers, B. Evaluation of organic coatings with electrochemical impedance spectroscopy. *JCT CoatingsTech* **2004**, *8*, 46−52.

https://doi.org/10.1021/acsomega.4c07098
ACS Omega 2025, 10, 18225−18237